INFRARED ANALYSIS OF THE TWO PHASE FLOW IN A SINGLE CLOSED LOOP PULSATING HEAT PIPE

Daniele Mangini, Marco Marengo
School of Computing, Engineering and Mathematics, University of Brighton, Lewes Road, BN2 4GJ Brighton, UK

Lucio Araneo
Politecnico di Milano, Energy Department, via Lambruschini 4A, Milano, Italy

Mauro Mameli*, Davide Fioriti, Sauro Filippeschi
DESTEC, University of Pisa, via Diotisalvi, Pisa, Italy
*mauro.mameli@ing.unipi.it

Abstract. A Single Loop Pulsating Heat Pipe (SLPHP) filled at 60% vol. with pure ethanol, having an inner diameter of 2mm, is designed with two sapphire tubes mounted between the evaporator and the condenser. Being the sapphire almost transparent in the infrared spectrum, such inserts allow simultaneous high-speed visualizations and infrared analysis of the fluid regimes. Two highly accurate pressure transducers measure the pressure at the two ends of one of the sapphire inserts. Three heating elements are controlled independently, in such a way to vary the heating distribution at the evaporator. It is found that particular heating distributions promote the slug/plug flow motion in a preferential direction, allowing to establish a self-sustained circulatory motion. It is demonstrated that a direct infrared visualization of the two-phase flow passing through the sapphire inserts is a valuable technique to measure the liquid slug bulk temperature after a proper calibration of the camera, with uncertainty of 1.5˚C (99.7% confidence level). Additionally, the fluid infrared visualization allows to appreciate the liquid film dynamics (wetting and dewetting phenomena) during the device operation, and to map the temperature gradients of liquid slugs thanks to the high-sensivity of the infrared measurements (0.05 K).

Keywords: Pulsating Heat Pipe, Infrared Analysis, Liquid film dynamics.

1. INTRODUCTION

As modern computer chips and power electronics become more powerful and compact, the need of more efficient cooling systems increases. In this scenario, Pulsating Heat Pipes (PHPs) are relatively new, wickless two-phase passive heat transfer devices that aim at solving thermal management problems mostly related to electronic cooling [1] [2]. Despite the advantages of this emergent technology, such as its compactness, the possibility to dissipate high heat fluxes and the ability to work also in microgravity conditions, the PHPs governing phenomena are quite unique and not completely understood [3]. Since the Single Loop PHP (SLPHP) can be considered the basic constituent of a multi-turn Pulsating Heat Pipe, its full thermo-fluidic characterization is fundamental for the complete description of the PHP working principles. At present, several studies already contribute to the understanding of SLPHP behaviour ([4], [5], [6], [7]), but further work is needed to have a clearer view on the thermo-fluid dynamics of the two-phase flow. Detecting quantitatively the liquid slug temperature with a non-intrusive technique is a mandatory step for a better comprehension of the PHP heat transfer phenomena. Additional efforts are also imperative to find new techniques able to describe the liquid film evolution during the device operation for the flow patterns usually observed within PHPs, i.e. the slug/plug flow and the semi-annular flow. In fact, being the Taylor flow the common flow pattern observed in PHPs, where vapor bubbles are surrounded by a liquid film deposited on the inner section of the tube wall, the analysis of the liquid film dynamics during the PHP operation is necessary in the understanding of the device fluid-dynamics and in the developement of further numerical models [8]. Also the most recent numerical modelling research [9] stresses the importance of the liquid film on the overall heat transfer performance, since the liquid film substantially influences the wall to fluid heat transfer rate and thus the simulated PHP behavior. Nevertheless, in this numerical work the liquid film thickness is assumed of constant thickness in space and time, assumption that is in contrast with the experimental work done by the same authors who examinated the liquid film generated by an oscillating meniscus within a single branch PHP [10]. The film shape is reconstructed using a well-known non-intrusive optical grid technique originally developed by Gurfein et al. [11]. The results indicate that the liquid film deposited during the liquid slug oscillation is not constant, being almost flat everywhere except showing a ridge at its end. The authors provides a valuable characterization of the liquid film only in the case of periodic flow oscillation which may not take into account the thermally induced non-periodic oscillation of the fluid typical of closed loop PHPs. Therefore, additional efforts are necessary to understand the liquid film dynamics also in a closed loop PHP geometry.

In the literature, different techniques have been already used with the common aim to experimentally investigate the internal thermo-fluid dynamics. In Gully et al. [12], micro-thermocouples and pressure transducers are positioned directly

in contact with the two-phase flow in a horizontal single branch stainless steel PHP. Quantitative measurements of the vapor bulk temperature and pressure are obtained. They find that the vapour is in superheated conditions. Due to the complexity of the experimental design, the authors cannot simultaneously visualize the flow during the experiments, and therefore no information regarding the fluid regimes is given.

High-speed visualization provides vital information regarding the intrinsic relationship between the flow motion and the parameters analyzed, showing the flow pattern transitions during the device operation. Therefore, high-speed visualization techniques are adopted to highlight the two-phase flow motion within the capillary tube, by varying the working fluids, the heating power levels [13] [14], the gravity field [15], [16] sometimes defining flow pattern maps [17], [18]. Rana et al. [19] performed a micro-PIV analysis focusing on the liquid-vapour interface behavior in a square capillary tube. The authors measured the liquid velocity near the meniscus and it was observed that the flow becomes tri-dimensional at the vapour/liquid interface. No information regarding the liquid film dynamics were reported.

Thanks to the technological improvement of the high-speed InfraRed (IR) cameras in terms of spatial resolution and acquisition frequency, IR imaging could represents a breakthrough for the non-intrusive analysis of the complex thermo-fluid dynamic occurring inside PHPs. The main advantages of the IR technique are the high sensitivity, non-intrusiveness and the low response time. Nevertheless, an in-situ calibration is mandatory, and the accuracy is still relatively low depending very much indeed the actual experimental conditions which may differ from the one adopted during calibration. As already pointed out by Hestroni et al. [20], care must be taken because of the numerous external radiation sources may alter the measurements. IR analysis was used in recent studies to measure quantitatively the external PHP wall temperatures ([21], [22], [23], [24], [25]). Nevertheless, a direct IR analysis of the fluid may be able to detect the liquid interface temperature and even the liquid film dynamics within the PHP tube. An important aspect is that the fluids used in PHPs are not fully opaque in the IR spectrum, therefore, the liquid global emissivity depends on the thickness. Sobac and Brutin [26] measured the relationhip between the global emissivity and the liquid thickness of several fluids, such as methanol, ethanol and FC-72 keeping constant the droplet temperature at 25˚C. The authors performed an IR analysis of an evaporating ethanol droplet positioned upon a heated suface with a Middle-Wave Infrared-Camera (MWIR camera) operating beween 1 μm and 5 μm. In the case of ethanol, the global emissivity tends asymptotically to 1 when the liquid thickness is greater than 2 mm, therefore, quantitative fluid temperature measurements can be accurate only when the liquid thickness is known a priori. Nevertheless, the authors calculate the emissivity of ethanol at 25˚C, and at the moment it is not investigated in the literature if, varying the liquid temperature in a certain range, the emissivity of such a fluid changes or not. This is a crucial point if one wants to calculate the liquid bulk temperature within a PHP partially filled up with ethanol using a MWIR camera. Being the PHP a two-phase heat transfer device, in which an efficient thermal exhchange is achievable by means of a self-sustained oscillating two-phase flow motion, of course the liquid temperature is not constant, and further analysis is needed to investigate the effect of the liquid temperature on the emissivity value.

Recently, Liu and Pan [22] performed IR measurements to estimate the heat transfer coefficient of the flow boiling in a capillary tube. The rectangular channel is made of germanium (transmittance in the infrared spectrum ranges between 85% and 95%) and it is filled up with ethanol. The error analysis shows an uncertainty of 13% of the temperature in °C. Since the experimental temperature range is between 30°C and 50°C, it means that the measurement uncertainty renges from 3,9 °C and 6,5°C and can be largely improved. Table 1 compares the different measurement techiques adopted so far in the literature to study experimentally the two phase thermo-fluid dynamics, showing with a dot symbol the ability to detect the liquid/vapor dynamic and to provide quantitative temperature measurements on the liquid phase, the vapor phase, the interface and the liquid film.

Table 1: Comparison between different measurement techiques that aim to study the thermofluid dynamics of PHPs.

Author	Geometry/ Cross section	Meas. Techniq.	Liquid phase		Vapor phase		Interface		Liquid film		
			Temperat.	Dynam.	Temperat.	Dynam.	Temperat.	Dynam.	Temperat.	Dynam.	Thick.
[10]	Single branch/ Rectang.	grid deflection method, interfero.		●				●		●	●
[12]	Single branch/ Circular	Micro TC	●		●						
[6]	Loop/ Rectang	Time strip visual.		●		●		●		●	
[22]	Flow boling /Square	IR on fluid	●	●		●		●		●	
Present work	Loop/ circular	IR on fluid	●	●		●		●		●	

This literature review shows that the direct IR analysis may be a suitable tool to identify the liquid film dynamics in PHPs. Moreover, synchronizing in time the IR images with fluid pressure measurements and high-speed images in the visible spectrum, it is possible to obtain a novel, accurate characterization of the slug/plug regimes.

In the present experiment, two transparent sapphire tubes connect the hot and the cold sections, allowing both high-speed visualization and IR analysis of the fluid flow. Two high precision pressure transducers, mounted at the ends of one sapphire insert, allow to measure the local fluid pressure. Three independent heaters are mounted on the evaporator section. The PHP is designed with an ID of 2 mm and it is partially filled up with ethanol. Therefore, when a liquid slug fills completely the sapphire tube, the liquid bulk temperature can be measured with a MWIR. A ground test characterization is performed, by varying the heating power distribution at the evaporator and showing that the flow circulation may be controlled providing specific heating distributions. The different flow patterns and the wetting/dewetting phenomena are analysed for the first time by means of a direct two-phase fluid IR analysis, providing useful information on the basic phenomena involved in PHP operation.

2. EXPERIMENTAL APPARATUS

The basic features of the actual SLPHP are shown in Figure 1a. The evaporator and the condenser are made of copper tubes (inner diameter 2 mm, outer diameter 4 mm) in order to minimize the thermal resistance between the tubes, the heat source and the heat sink. They are connected to two sapphire tubes (110 mm axial length, trasmissivity 0.9), having the same inner and outer diameter of the copper tubes, by means of brass joints, designed to maintain the flow path shape continuity, and glued by means of epoxy for vacuum applications (Henkel Loctite® 9492). Two high accuracy pressure transducers (Keller® PX33, 1 bar absolute, accuracy 0.05%), mounted at the ends of one sapphire insert, measure the pressure drop along the adiabatic section (190 mm axial length). The condenser section is embedded inside a mini shell and tube heat exchanger, connected to a thermal bath (Lauda® A300), that recirculates water at 20°C ±1 °C. The high-speed camera (Ximea® USB3 XIQ-093, resolution 1280x1024 pixel) records images up to 400 fps, while an high-speed and high resolution Medium Wave IR Camera (AIM® from TEC-MMG, spatial resolution 1280x1024, 50 fps, resolution ±0.05 K, bandwidth 3-5μm, lens transmissivity 0,93) records images at 50 fps for 20 consecutive seconds. The SLPHP is firstly evacuated with an ultra-high vacuum system (Varian® DS42 and TV81-T) down to 0.3 mPa and then partially filled with ethanol, degassed by continuous boiling and vacuuming cycles, as described by Henry et *al.*, 2004 [27], with a volumetric ratio of 0.6 ± 0.025 corresponding to 1.45 ml. Finally, the micro-metering (Microcolumn®, UP447) valve that connects the SLPHP to the device is closed (the leak rate of the selected valve is lower then 10^{-6} mbar l/s). Ethanol is chosen for its radiative properties in the MWIR spectrum: note that quantitative temperature measurements can be achieved when the liquid slug completely fills the capillary tube of the device. Three heating wires (Thermocoax®, Single core 1Nc Ac) are mounted on the evaporator section, providing a nominal wall-to-fluid heat flux of 6.5 W/cm^2 at 10 W. The heaters are controlled independently with a Pulse Width Modulation (PWM) control system, so as to vary the heating distribution along the heated zone. As shown in Fig. 2a, two heating elements (Heater A and Heater C) are positioned just above the 90° curves at the evaporator, to heat up the device non-symmetrically with respect to the gravity field, while the Heater B is mounted in the middle of the evaporator horizontal section. As already demonstrated [28], heating up the device non-uniformly and non-symmetrically with respect to the gravitational force, a circulation in a preferential flow circulation may be established. This improves the overall thermal performance and allows to vary and control the flow patterns to be analysed by the IR camera. Twelve T-type thermocouples measure the external wall temperature both in the heated and in the cooled region of the single loop (see *Figure 1*b), while other two thermocouples monitor the ambient temperature. The thermocouples that record the temperatures in the evaporator (respectively, TC1 and TC2 for the Heater A; TC3 and TC4 for the HeaterB; and TC5and TC6 for the Heater C) are positioned as close as possible to the heating elements (maximum distance of 5 mm from the edge of the heating element). An additional thermocouple is placed on the back screen (TC_{bs} in *Figure 1*b), with the aim to control the temperature of the surface behind the sapphire insert. The back screen is a heat exchanger plate, in which de-ionized water is continuously flowing. The temperature of the de-ionized water is controlled by means of a Peltier system (Adaptive®, ETH-127-14-11-S, Merstetter Eng. ® TEC-1123) that keeps it constant at 20˚C ±1˚C. The SLPHP, together with the MWIR camera, are positioned in a black painted box with the purpose to avoid radiation noise from the environment. The overall system is designed with the aim to decrease as maximum as possible the dead volumes that can affect the flow motion and thus the overall performance of the system. Indeed, the dead volumes represent the 2% of the overall volume of the SLPHP. A data acquisition system (NI-cRIO-9074®, NI-9264®, NI-9214®, 2xNI-9205®, NI-9217®, NI-9472®) records the thermocouples signal at 10 Hz, and the pressure transducers signal at 100 Hz. The high-speed camera is connected to an ultra-compact PC (NUC® Board D54250WYB) able to store images up to 100 fps, which is synchronized via software with the pressure signals.

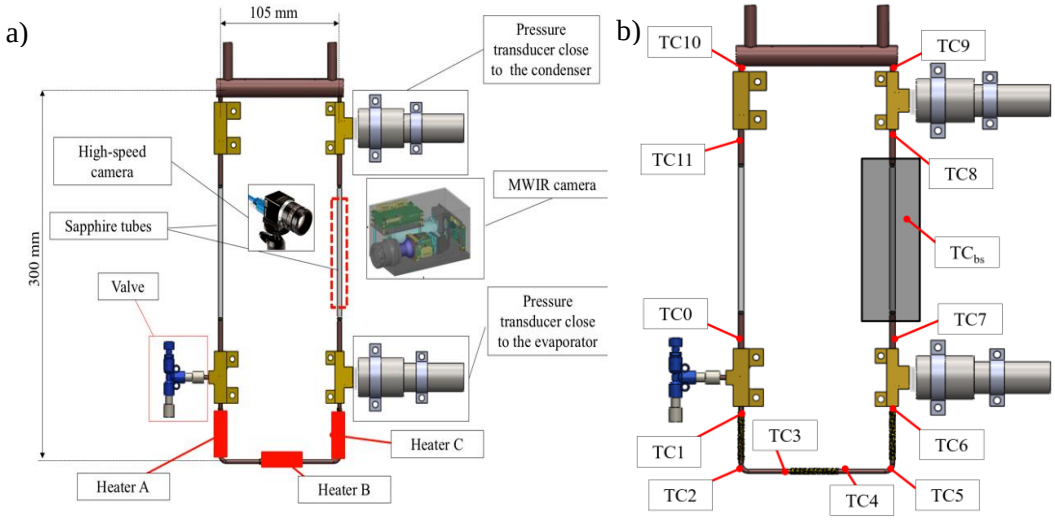

Figure 1. a) Main components of the system:the sapphire section where both the high-speed visualization and the IR analysis are performed is red dashedwhilethe heating elements are red; b) Thermocouple positions.

3. EXPERIMENTAL RESULTS AND PROCEDURE

3.1. Thermal performance and fluid regimes

Tests are performed maintaining the ambient temperature at 20°C±1°C, and positioning the device vertically in Bottom Heated Mode (BHM), i.e. with the evaporator section below the condenser. The heating power is increased from 9 W up to 30 W. Pseudo steady state conditions (i.e. until the mean evaporator tube wall temperature achieves a constant value) can be usually reached after approximately three minutes, due to the low thermal inertia of the system. Nevertheless, all the heating configurations have been kept for 15 min. A video sequence (20 s at 100 fps) is recorded with the high-speed camera. The video acquisition starts 13 min after each heat input power variation. The equivalent thermal resistance (R_{eq}) is evaluated as follows:

$$R_{eq} = {(\bar{T}_e - \bar{T}_c)}/{\dot{Q}_{tot}} \qquad \text{(Eq. 1)}$$

where $\bar{T}_e, \bar{T}_c$ are respectively the average of the temperatures at the evaporator and at the condenser when pseudo steady state conditions are reached, while $\dot{Q}_{tot}$ is the global heating power. Being the three heating elements in series, the global heating power is the sum of the heating power dissipated by the Heater A ($\dot{Q}_A$), Heater B ($\dot{Q}_B$)and Heater C ($\dot{Q}_c$):

$$\dot{Q}_{tot} = \dot{Q}_A + \dot{Q}_B + \dot{Q}_C \qquad \text{(Eq.2)}$$

Since each of the three heating elements, being controlled independently, can provide different heating powers, the $\bar{T}_e$ is:

$$\bar{T}_e = \frac{\dot{Q_A}}{\dot{Q_{tot}}}\max(T_1;T_2) + \frac{\dot{Q_B}}{\dot{Q_{tot}}}\max(T_3;T_4) + \frac{\dot{Q_C}}{\dot{Q_{tot}}}\max(T_5;T_6) \qquad \text{(Eq. 3)}$$

The higher temperatures close to the heating elements is selected in order to provide the overall heat transfer performance of the device in the most cautelative condition. The temperature at the condenser, $\bar{T}_c$ is simply the average between the thermocouples TC9 and TC10. The heating power is increased from 1 W to a global power of 30 W, varying the heating distribution along the three heating elements and testing different heating configurations according to Table 2.

Table 2: Heating configurations

Config.	HEATER A [W]	HEATER B [W]	HEATER C [W]
1	6	3	0
2	9	9	0
3	12	12	0
4	15	15	0

The temporal trend of the temperatures and the pressures at the evaporator side, and all the heating configurations are shown in *Figure 2*.

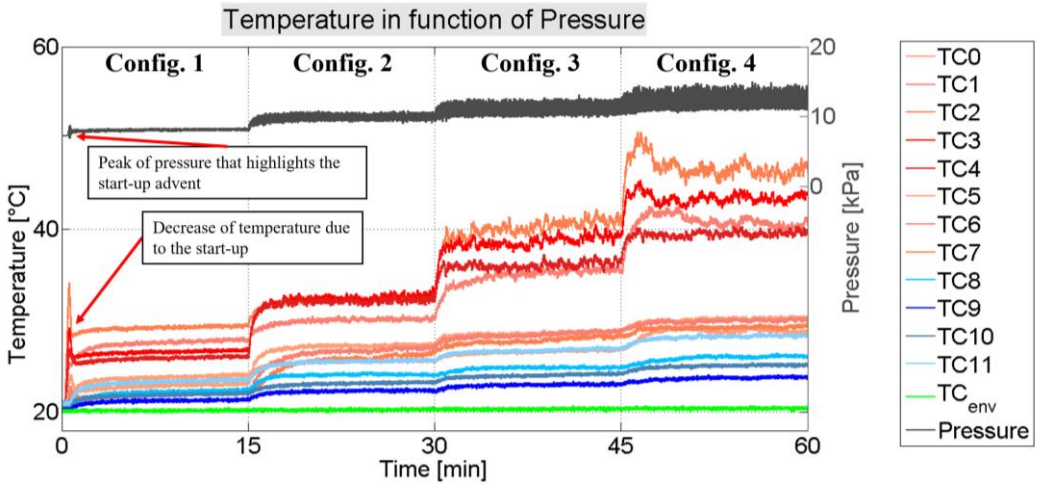

Figure 2. Temperatures and pressure evolution during the long-time test.

The start-up is detectable at 9 W (Config. 1): a sudden peak of pressure is recorded by the transducer mounted at the evaporator, while at the same time the temperatures in the heated zone suddenly decrease, remaining constant thereafter between 30˚C and 35 ˚C. A clear circulation of the two-phase flow in a preferential direction is observable through the two transparent sections. The visualization shows a semi-annular flow in the left transparent section, moving from the evaporator to the condenser, while a slug/plug flow comes down through the right transparent insert. The fact that the flow is circulating in a preferential direction is due to the peculiar heating configuration provided at the evaporator [28]. The local heating power dissipated by the Heaters A and B preferentially pushes the fluid through the left branch of the device (Up-header). In this channel a semi-annular flow is observable (*Figure 3*). Then, due to the coupled effect of condensation and gravity head, the flow returns with a lower temperature from the condenser to the evaporator through the right side of the SLPHP (Down-comer). A better control of the flow motion and the flow pattern is reached with a non-symmetrical heating configuration. In this case the liquid slugs fill completely the tube section and, therefore, their maximum liquid thickness is constant and equal to the internal tube diameter (2 mm).

The circulation of the flow motion in a preferential direction can be deduced also by the temporal evolution of the temperature measured by the thermocouple TC10 and the temperature measured by the thermocouple TC9: the hot fluid coming from to the evaporator towards the condenser through the left channel, passes by TC10 and then it is cooled down by the condenser before passing by TC9. This is valid for all the heating configurations provided during the test.

a)

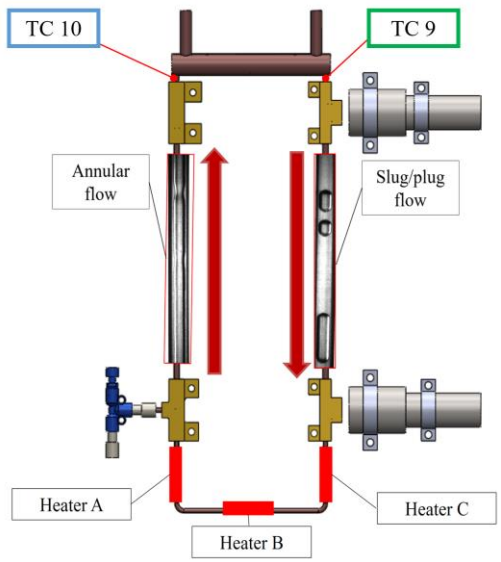

b)

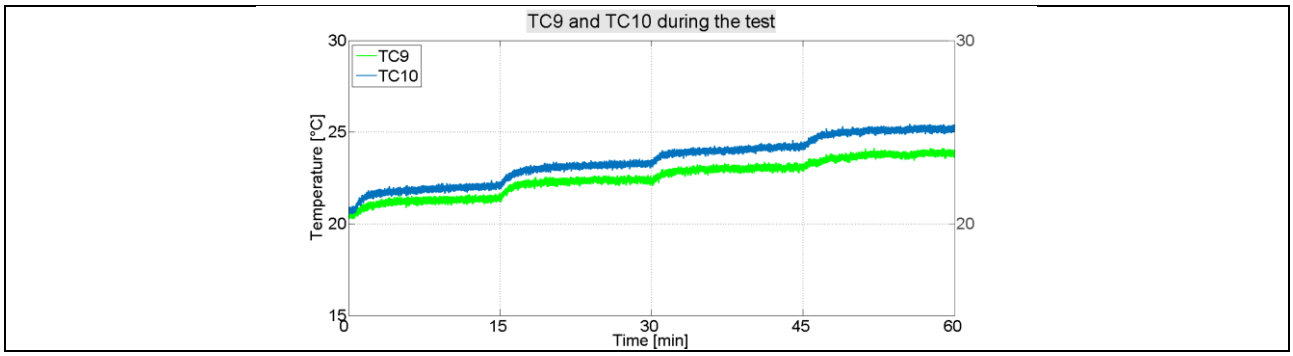

Figure 3. a) Annular flow in the up-header and slug/plug flow in the down-comer; b) temporal evolution of the temperatures at the condenser during the test.

The Equivalent Thermal Resistance value is lower than 1 K/W for all the heating configurations (Figure 5). The non-symmetrical heating power provided during tests, stabilizing the flow circulation in a preferential direction, enhances the overall performance of the device, as already highlighted [28]. Such a two-phase flow motion in a preferential direction improves the overall performance by continuously refreshing the hot section with a fluid flow that comes from the condenser with a lower temperature.The device dissipates efficiently heat also providing 30 W (Config. 4), keeping the R_{eq} below 0.7 K/W.

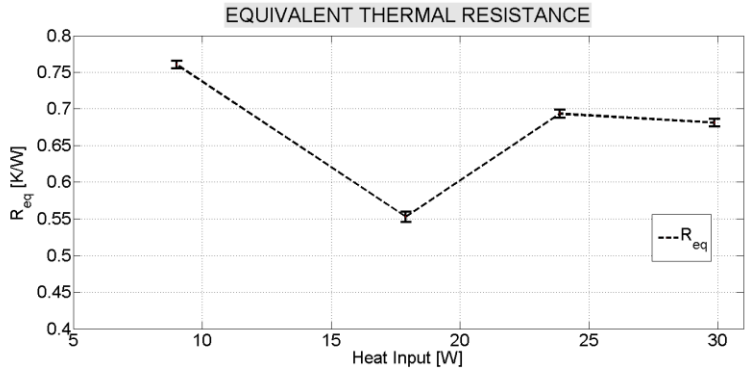

Figure 4. Equivalent Thermal Resistance Value for the different heating configurations.

3.2. IR analysis

The IR-camera has been calibrated by developing and running a separate liquid loop (*Figure 5*) built with the same sapphire tube mounted on the PHP. The sapphire tube is connected to a thermal bath (Lauda ECO®) to recirculate the pure ethanol vary its temperature. Two thermocouples measure the inner and the outlet fluid temperature (T-type thermocouples, maximum error 0.4K). The tube and the IR-camera are both positioned in a black painted box. During the calibration procedure, the room temperature was kept constant at 20˚C ± 1˚C. The fluid temperature is varied by means of the thermal bath from 15°C to 50°C, with steps of 5°C. As soon as the system reaches the steady state, both the thermocouple signals (5Hz for 20s) and the IR images (20s at 50fps) are recorded. A MatLab® code is developed to establish a correlation between the radiative emission coming from the tube and the fluid temperatures by means of a fith order polynomial fitting:

$$T_f = p_1 N_{cam}^4 + p_2 N_{cam}^3 + p_3 N_{cam}^2 + p_4 N_{cam} + p_5 + \varepsilon \qquad \text{(Eq. 4)}$$

where T_f is the fluid temperature, N_c the reading from the camera, p_1-p_5 the coefficients of the polynomial, and ε a residual error.

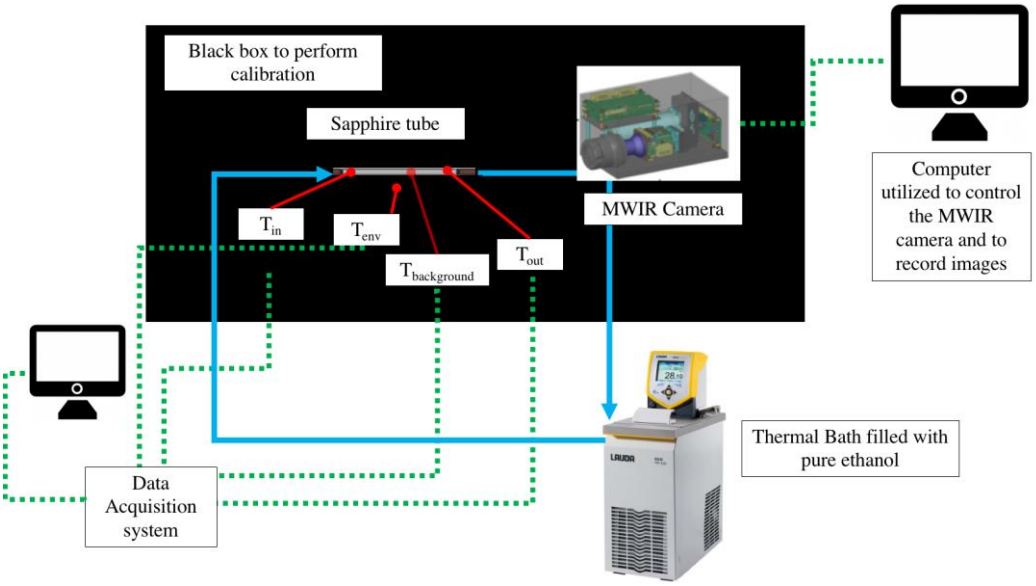

Figure 5. Schematizayion of the experimental apparatus to perform the MWIR calibration.

The methodology adopted for the uncertainty analysis calculates the expected value and the standard uncertainties, i.e. the estimated standard deviations, of the calibration coefficients of the polynomial through a Monte Carlo approach, as proposed in the Guide to the expression of uncertainty in measurement [29]. Moreover, the final uncertainty of the fluid temperature $u(T_f)$ is calculated by applying the procedure of the GUM to Equation 4:

$$u(T_f)^2 = \left(\frac{\partial T_f}{\partial N_{cam}}\right)^2 u(N_{cam})^2 + \sum_{i=1}^{5}\left\{\left(\frac{\partial T_f}{\partial p_i}\right)^2 u(p_i)^2 + \sum_{j=i+1}^{5}\left[2corr_{i,j}\left(\frac{\partial T_f}{\partial p_i}\right)\left(\frac{\partial T_f}{\partial p_j}\right)u(p_i)u(p_j)\right]\right\} + u(\varepsilon)^2 \quad \text{(Eq. 5)}$$

where $corr_{i,j}$ is the correlation ratio between uncertainties of the polynomial coefficients evaluated by the Monte Carlo approach; $u(N_c)$, $u(p_i)$, and $u(\varepsilon)$ are the uncertainties of the camera signal, the polynomial coefficients, and the residual error, respectively. The uncertainties of any measured quantity take into account both the intrinsic error of the instrument (type b uncertainty u_b), and the quantity related to the repeated measurements (type a uncertainty u_a), as in Equation 6:

$$u(X) = \sqrt{u_a^2 + u_b^2} \quad \text{(Eq. 6)}$$

The maximum errors of the used instrumentations are 0.4 K for the thermocouples signal and 5 digits for the camera signal. The type B uncertainties are calculated assuming an uniform probability density (function of the errors for both temperature and camera readings), as suggested in the Guide to the expression of uncertainty in measurement [30]. The final calibration curve, the standard uncertainties calculated with the procedure described above, and the experimental points are depicted in *Figure 6*. The calculated expanded uncertainty is 1.5˚C, with a level of confidence of 99.7%.

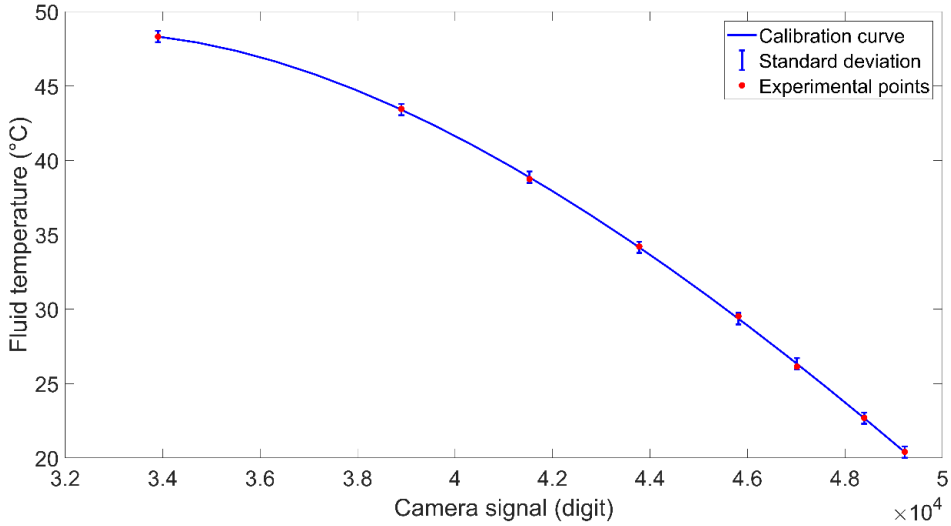

Figure 6. Calibration curve of ethanol (constant thickness of 2 mm) and the related error for all the temperatures tested.

An additional calibration is performed with a black body and the same MWIR camera. The aim of such an additional calibration is to investigate if ethanol can be considered opaque in the temperature range achieved during tests in the sapphire insert (from 20˚C to 35˚C), keeping constant its thickness at 2 mm. This is done because no information about the emissivity of ethanol at different temperature levels are present in the literature, to the author`s best knowledge. Indeed, in the previous work done by Sobac and Brutin [26], the emissivity of such a fluid was calculated keeping constant the liquid droplet at 25˚C. The black-body enclosure is designed following the guidelines provided by Quinn [31]. The black body (emissivity 0.997) is a copper tube, with a inner diameter of 30 mm and with an axial length of 280 mm. It is equipped with 4 T-type thermocuples and one PT 100 (classA, accuracy 0.19˚C), that records the wall tube temperature during the calibration. The black body is wrapped with a silicon serpentine (ID 5 mm, OD 7 mm), in which water at a constant temperature is flowing continuously. The water temperature is controlled by means of the same Peltier system described in section 2. The black body is thermally insulated with 70 mm of low-conductive foam (0.1 W/mK thermal conductivity). The temperature of the black body is varied from 10˚C up to 45˚, with steps of 5˚C. The environmental temperature is kept constant at 20˚C±1˚C, and recorded with an additional PT 100 during the calibration. When steady state conditions are reached, both the temperatures recorded by the thermocuples and a sequence of 100 IR images are acquired. The calibration curves of the black body and the pure ethanol one are then compared. As shown in *Figure 7*, the maximum difference detected is less than 0.7K at 34˚C, comparable with respect to the standard deviation declared.

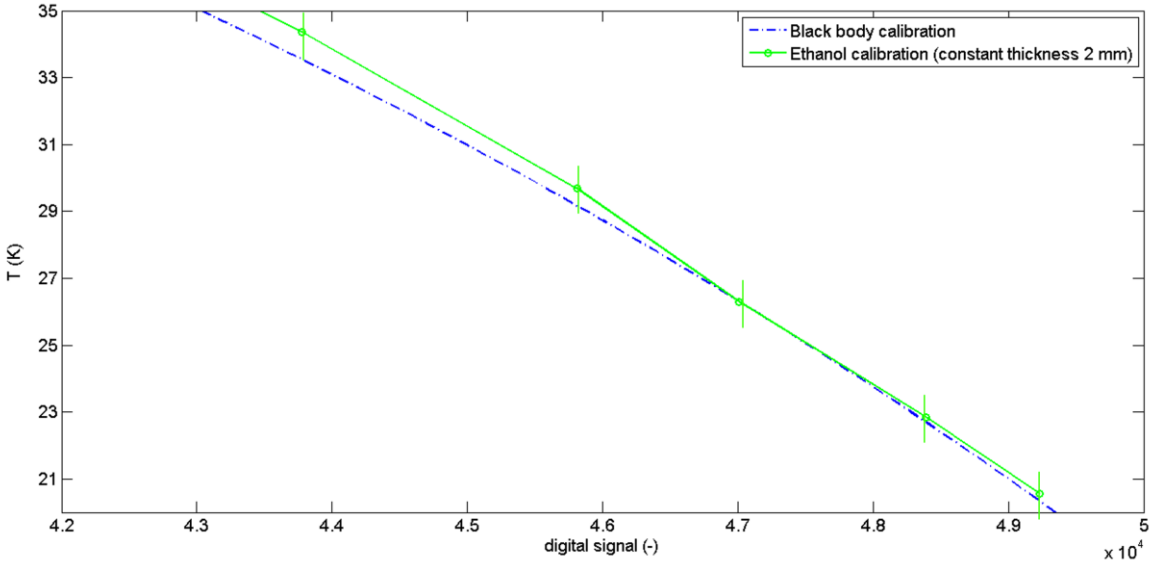

Figure 7. Comparison between the calibration curve obtained with pure ethanol (green), and the calibration curve obrained with a black body (red line) varying the temperature between 15 ˚C and 35 ˚C.

Pure ethanol can be considered opaque when a liquid slug fills completely the tube during experiments, from a range of temperature between 10 ˚C and 35 ˚C . Therefore, the radiosity (R in Eq. 7) of ethanol can be assumed equal to the radiation of the black body (E_{bb} in Eq. 7):

$$R = E_{bb} \quad \text{(Eq. 7)}$$

Applying the calibration curve to the IR images of the tests performed on the SLPHP, and comparing the corresponding liquid slug temperatures with respect to the signals recorded by the TC8 and the TC7 (respectively the two thermocuples located on the external wall temperature 10 mm before and after the sapphire tube) when pseudo steady state conditions are reached, the liquid temperature varies in the same temperature range (*Figure 8*). Focusing on the IR image, it can be noticed that the MWIR camera detects correctly the liquid slug temperatures along the sapphire insert. This is valid for the liquid phase, when the liquid plug fills completely the inner section. In the presence of vapor bubbles, being the vapor phase transparent in the IR-spectrum, the IR camera detects locally a lower temperature, being the T_{bs} set at 20˚C during tests.

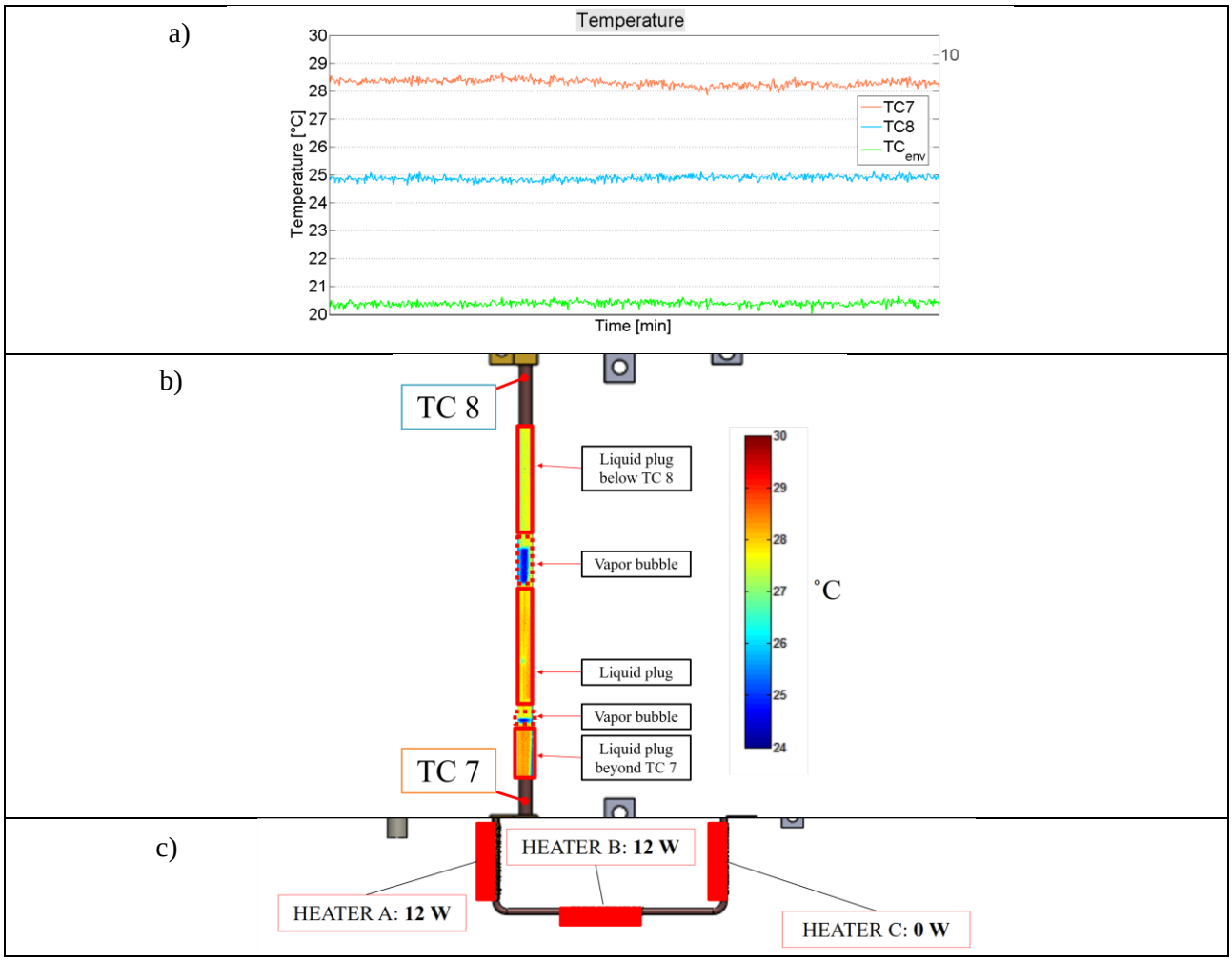

Figure 8 a) Temperatures evolution of TC7 and TC8 during tests, when pseudo-steady state conditions are reached; b) IR images after calibration.

In case of annular flow, the IR analysis could be utilized to provide quantitative measurements on the liquid film thickness too, even if further efforts needs to be done to prove it. In fact, in such a case the emissivity ε is a function of its thickness. At this stage, in case of annular or semi-annular flow, the IR visualization can be considered an useful tool to appreciate the liquid film dynamics during the PHP operation (*Figure 9*a). In order to obtain an annular flow in the sapphire insert in front of the IR camera, the heat is dissipated by the heating element just below the sapphire insert (*Figure 9*c). When the liquid film thickness is higher, the IR camera measures higher temperatures, being the emissivity directly proportional to the liquid film thickness.

a)

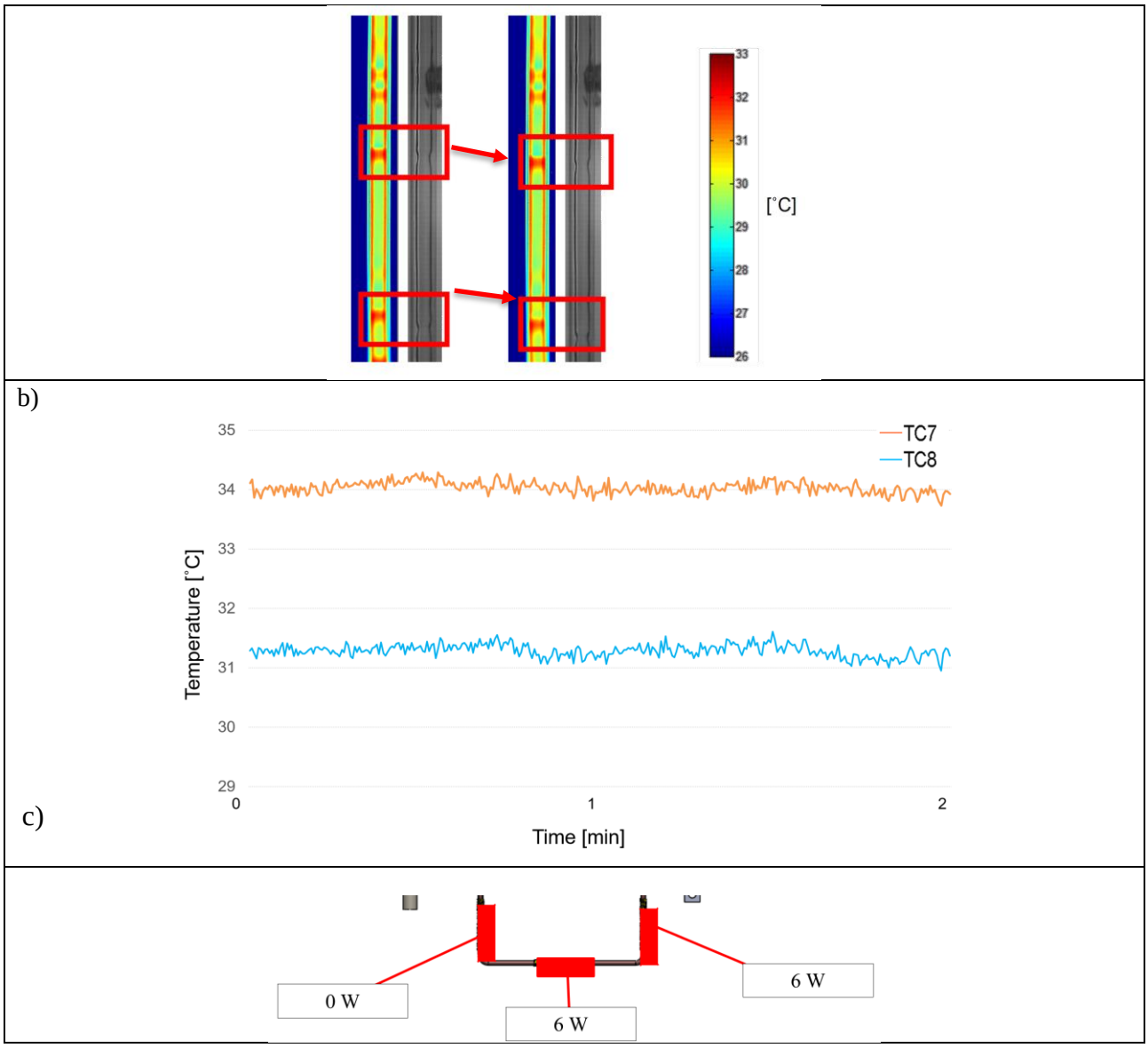

Figure 9. a) Two consecutive images temporally spaced at 0.02 ; b) Temperature evolution of TC7 and TC8; c) Heating configuration provided.

Wetting phenomena can be recognized with the direct IR analysis, too (*Figure 10*). During the start-up, the liquid temperature close to the evaporator starts to increase. The slug/plug flow motion is initially oscillating in the sapphire insert. During the first seconds, only some slug/plug oscillations are detectable (first two images in *Figure 10*). Such oscillations become more and more vigorous, until an intense acceleration of the two-phase flow changes the flow pattern from a slug/plug flow to a semi-annular flow (third and fourth images in *Figure 10*), and finally to an annular flow (last two images in *Figure 10*). As soon as the annular flow is detectable in the sapphire section, the variation of temperature between the tube ends become smaller and the liquid film wets the entire inner tube surface.

a)

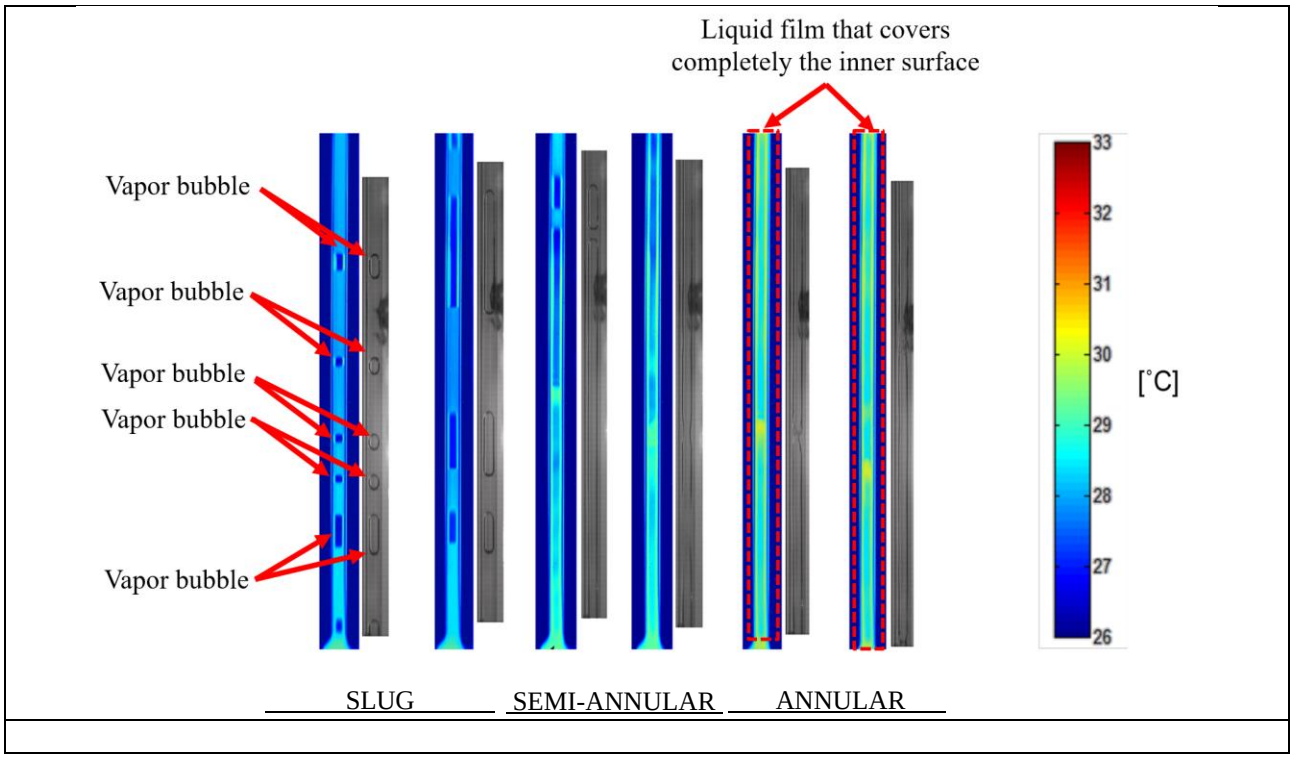

Figure 10. a) More relevant events observed during the start-up providing to the device a local heating power Heater A = 0W, Heater B = 6W, Heater C = 6W.

When semi-annular flow rises from the evaporator to the condenser, the liquid film may slide from the cooled to the heated section by gravity as shown in *Figure 11*b, similarly to two-phase thermosyphons. The sequence of images in *Figure 11*b is also synchronized with the two fluid pressure signals recorded at the ends of the sapphire insert. When the pressure does not show significant fluctuations, a liquid film sliding from the condenser to the evaporator is clearly observable thorugh the images obtained with the IR camera. As soon as both the pressure signals exhibit a significant fluctuation of 1.5 kPa (*Figure 11*c) the liquid film is pushed upwards.

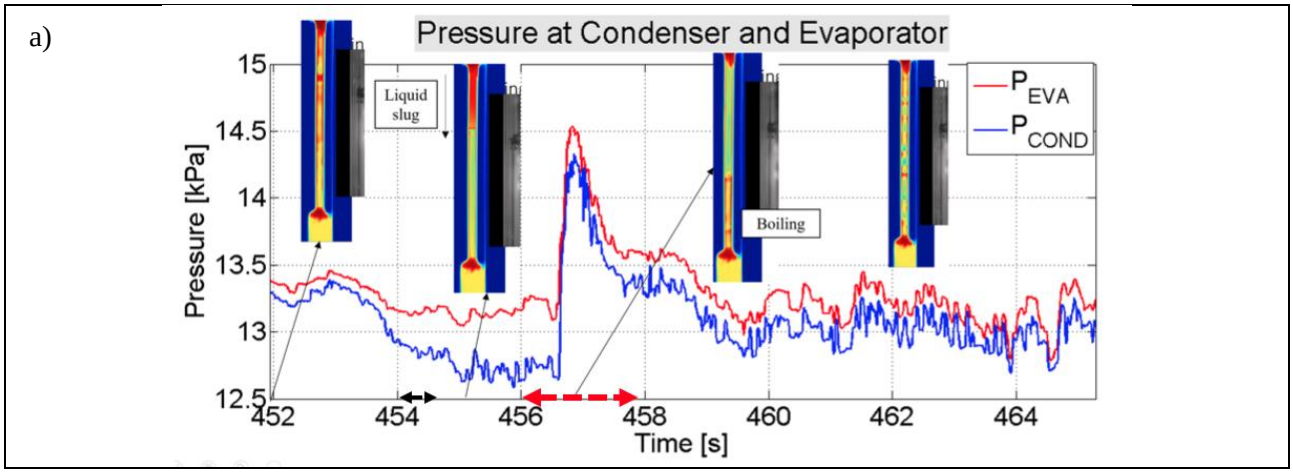

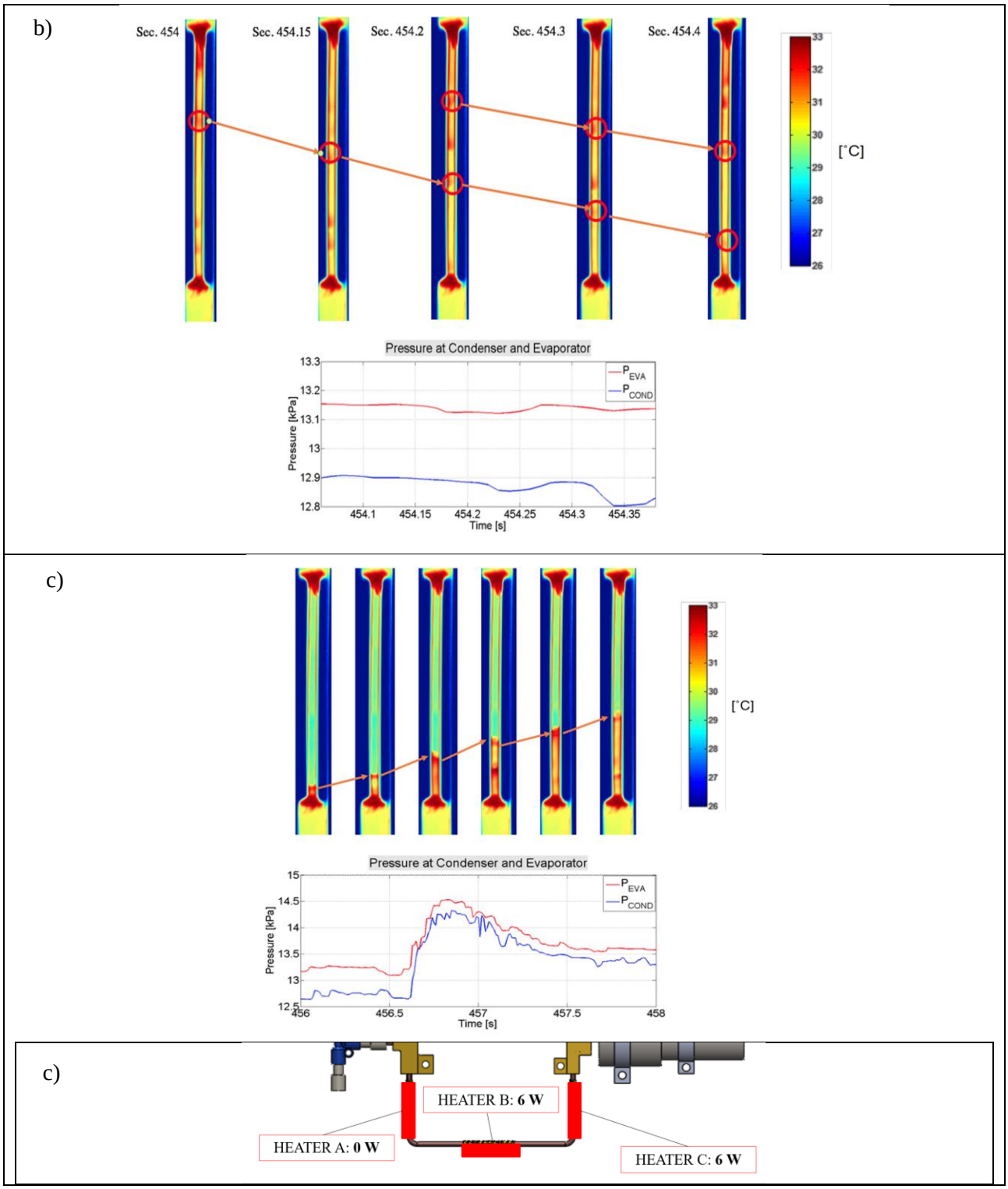

Figure 11. a) Synchronized pressure signals and IR images for oscillating flow. b) Zoom at t= 454s; c) Sequence of image at 50 fps at at t= 454s (i.e. during the pressure peak); c) the heating configuration.

Note that this phenomenon could not be detected by means of a standard CCD camera. Temperature gradients along the liquid slugs can be also appreciated too, thanks to the high sensitivity of the IR camera (0.05 K). *Figure 12*a shows a liquid slug pushed from the condenser to the evaporator providing to the device the heating configuration highlighted in *Figure 12*b. Interestingly, the higher temperature is initially close to the cooled section. This is due to the peculiar heating configuration provided to the evaporator: the flow is pushed from the left-branch in the form of annular flow with a higher temperature, and then pushed back by the coupled effect of gravity and condensation phenomena in the condenser in the right-branch. The gradient of temperature measured by the IR camera in this situation is 4 K along the slug. Subsequently,

as soon as the liquid plug approaches the evaporator, the temperature increases also in the lowest part of the slug, therefore decreasing the gradient of temperature.

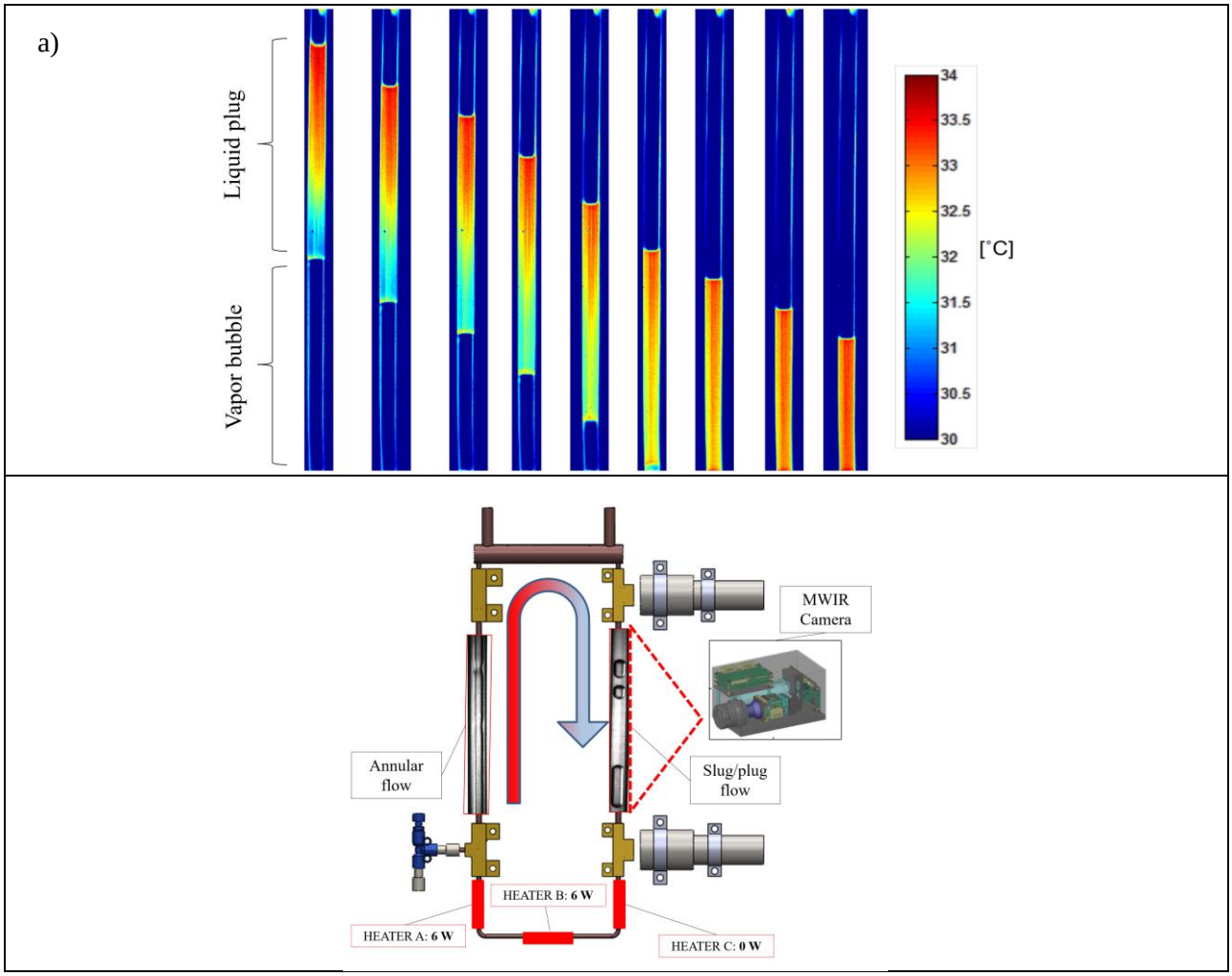

Figure 12.a) Sequence of image at 25 fps; b) heating configuration provided.

4. CONCLUSIONS

A Single Loop Pulsating Heat Pipe with a 2 mm inner diameter, filled with pure, degassed ethanol (60% FR), is tested in Bottom Heated Mode. The total heating power, as well as the heating configuration at the evaporator, is changed during tests by means of three heating elements independently controlled. With respect to previous SLPHP experiments in literature, such a device is designed with two sapphire inserts mounted between the evaporator and the condenser. The sapphire, being almost transparent in the Infrared spectrum, allows a IR analysis of the inner two-phase flow motion. A robust calibration method based on a secondary liquid temperature controlled loop is proposed and compared with the black body standard calibration. The polynomial fitting of the fluid temperature is also passed through a montecarlo uncertainty analysis, showing that the direct IR temperature measurement of an opaque liquid (i.e. ethanol) is possible with a maximum error of ± 1.5˚C, (99.7% confidence level). Moreover, together with the synchronized images recorded by a high-speed camera, the proposed technique is able to detect the wetting and de-wetting of the liquid film which cannot be observed by a standard CCD camera. An axial temperature gradient of 4 K could be measured along a liquid slug during the actual PHP operation. The data obtained with the IR analysis of real PHP operations could provide useful information for the validation of PHP lumped parameters models ([9], [32]) and the novel CFD simulations ([33], [34]).

ACKNOWLEDGEMENTS

The present work is carried forward in the framework of two projects: the Italian Space Agency (ASI) project ESA_AO-2009 DOLFIN-II and the ESA MAP Project INWIP. We would like to thank particularly Ing. Paolo Battaglia (ASI) for his support and all the great NOVESPACE team in Bordeaux, Dr. Olivier Minster and Dr. Balazs Toth for their

interest and support to our PHP activities. Furthermore, the team would like to thank the TRP project and the laboratory TEC-MMG at ESA/ESTEC which borrows us the MWIR camera utilized in this work.

NOMENCLATURE

R_{eq}	Equivalent thermal resistance (K/W)
T	Temperature (ºC)
$\dot{Q}$	Heat Input power (W)
R	Radiosity (W/m^2)
E	Emissivity (W/m^2)
ε	Residual error (-)
u	Uncertainty (-)
p	Coefficient of the polynomial (-)

Subscripts

A	First heater
B	Second heater
C	Third heater
c	Condenser
e	Evaporator
tot	Total
bs	Backscreen
bb	Black Body
f	fluid
cam	camera

REFERENCES

[1] H. Akachi, Structure of a heat pipe US Pantent 4.921.041, 1990.

[2] H. Akachi, Structure of a micro heat pipe US Patent 5.219.020, 1993.

[3] Y. Zhang and A. Faghri, Advances and unsolved issues in pulsating heat pipes, Heat Transf. Eng. 29 (2008) 20-44.

[4] S. Khandekar and M. Groll, An insight into thermo-hydrodynamic coupling in closed loop pulsating heat pipes, Int. J. Therm 43 (2004) 13-20.

[5] S. Khandekar, A. Gautam and P. Sharma, Multiple quasi-steady states in a closed loop pulsating heat pipe, Int. J. Therm. Sci. 48 (2009) 535-546.

[6] G. Spinato, N. Borani and J. Thome, Understanding the self-sustained oscillating two-phase flow motion in a closed loop pulsating heat pipe, Energy 90 (2015) 889-899.

[7] G. Spinato, N. Borani and J. Thome, Operational regimes in a closed loop pulsating heat pipe, Int. J. Therm. 102 (2016) 78-88.

[8] V. Nikolayev, A dynamic liquid film model of the pulsating heat pipes, J. Heat Transf. 133 (2011).

[9] I. Nekrashevych and V. Nikolayev, Effect of tube heat conduction on the pulsating heat-pipe start-up, Appl. Therm. Eng. 117 (2017) 24-29.

[10] L. Forgeaud, L., Nikolayev, V., Ercolani, E., Duplat, J., Gully, P., In situ investigation of liquid films in pulsating heat pipes. Appl Therm Eng 126 (2017) 1023-1028

[11] V. Gurfein, D. Beysens, Y. Garrabos and B. Neindre, Simple grid technique to measure refractive index gradients, Opt. Commun. 85 (1991) 147-152.

[12] P. Gully, Evaluation of the vapour thermodynamic state in PHP, in 17th Int. Heat Pipe Conf., Kanpur, India, (2013).

[13] Y. Zhang, J. Xu and Z. Zhou, Experimental study of a Pulsating Heat Pipe using FC-72, Ethanol and water as working fluids, Exp. Heat Transf. 17 (2004) 47-67.

[14] L. Xu, Y. Li and T. Wong, High speed flow visualization of a closed loop pulsating heat pipe, Int. J. Heat Mass Trans. 48 (2005) 3338-3351.

[15] D. Mangini, M. Mameli, A. Georgoulas, L. Araneo, S. Filippeschi and M. Marengo, A pulsating heat pipe for space applications: ground and microgravity experiments, Int. J. Therm. Sci. 95 (2015) 53-63.

[16] D. Mangini, M. Mameli, D. Fioriti, S. Filippeschi, L. Araneo and M. Marengo, Hybrid Pulsating Heat Pipe for space applications with non-uniform heating patterns: ground and microgravity experiments, Appl. Therm. Eng.,126 (2017) 1029-1043.

[17] N. Saha, P. Das and P. Sharma, Influence of process variables on the hydrodynamics and performance of a single loop pulsating heat pipe, Int. J. Heat Mass Tran. 74 (2014) 238-250.

[18] M. Mameli, D. Mangini, G. Vanoli, L. Araneo, S. Filippeschi and M. Marengo, Advanced multi-evaporator loop thermosyphon, Energy 112 (2016) 562-573.

[19] G. Rana, T. Sahu, S. Khandekar and P. Pangrahi, Hydrodynamics of a confined meniscus in a capillary tube, in Proc. of 16th Int. Heat Pipe Conference (16th IHPC), Lyon, France, 2012.

[20] G. Hestroni, A. Mosyak, E. Pogrebnyak and R. Rozenblit, Infrared temperature measurement in micro-channels and micro-fluid systems, Int. J. Therm. Sci. 50 (2011) 853-868.

[21] V. Hemadri, A. Gupta and S. Khandekar, Thermal radiators with embedded pulsating heat pipes: infra-red thermography and simulations, Appl. Therm. Eng. 31 (2011) 1332-1346.

[22] T. Liu and C. Pan, Infrared thermography measurement of two-phase boiling flow heat transfer in a microchannel, Appl. Therm. Eng. 94, (2016) 568-578.

[23] V. Karthikeyan, S. Khandekar, B. Pillai and P. Sharma, Infrared thermography of a pulsating heat pipe: flow regimes and multiple steady states, Appl. Therm. Eng. 61 (2013) 470-480.

[24] V. Karthikeyan, S. Khandekar, B. Pillai and P. Sharma, Infrared thermography of a pulsating heat pipe: flow regimes and multiple steady states, Appl. Therm. Eng. 62 (2014) 470-480.

[25] N. Chauris, V. Ayel, Y. Bertin and C. Romestant, Evaporation of a liquid film deposited on a capillary heated tube: experimental analysis by infrared thermography of its thermal footprint, Int. J. Heat Mass Trans. 86 (2015) 492-507.

[26] B. Sobac and D. Brutin, Thermocapillary instabilities in an evaporating drop deposited onto a heated substrate, Ph Fluid 24 (2014).

[27] C. Henry, J. Kim and B. Chamberlain, Heater size and heater aspect ratio effects on sub-cooled pool-boiling heat transfer in low-g, in 3rd International Symposium on Two-Phase Flow modeling and Experimentation (2014), Pisa, Italy.

[28] A. Ilinca, D. Mangini, M. Mameli, D. Fioriti, S. Filippeschi, L. Araneo, N. Roth and M. Marengo, Fluid-flow pressure measurements and thermo-fluid characterization of a single loop two-phase passive heat transfer device, J. Phys.: Conf. Ser. 923 012022 (2017).

[29] (The) Joint of Metrology, Supplement 1 to the Guide to the expression of uncertainty in measurement, Propagation of distributions using a Monte Carlo method, 101: 2008.

[30] (The) Joint of Metrology, Evaluation of measurement data to the Guide to the expression of uncertainty in measurement., 100:2008.

[31] T. Quinn, The calculation of the emissivity of cylindrical cavities giving near black-body radiation, J. Appl. Therm. Phys. 18 (1967).

[32] M. Manzoni, M. Mameli, C. d. Falco, L. Araneo and M. Marengo, Advanced numerical method for a thermally induced slug flow: application to a capillary Closed Loop Pulsating Heat Pipe, Int. J. Num. Meth. Fluids 82 (2016) 375-397.

[33] S.M. Pouryoussefi and Y. Zhang, Numerical investigation of chaotic flow in a 2D closed-loop pulsating heat pipe, Appl. Therm. Eng. 68 (2015) 617-627.

[34] E. Jiaqiang, X. Zhao, Y. Deng and H. Zhu, Pressure distribution and flow characteristics of closed oscillating heat pipe during the starting process at different vacuum degrees, Appl. Therm. Eng. 93 (2015) 166-173.

365
366